Gas-flow animation by unsteady heating in a microchannel

A. Manela[1,a)] and N. G. Hadjiconstantinou[2]
[1]*Department of Mathematics, Massachusetts Institute of Technology, Cambridge, Massachusetts 02139, USA*
[2]*Department of Mechanical Engineering, Massachusetts Institute of Technology, Cambridge, Massachusetts 02139, USA*

(Received 2 February 2010; accepted 7 May 2010; published online 18 June 2010)

We study the flow-field generated in a one-dimensional wall-bounded gas layer due to an arbitrary small-amplitude time variation in the temperature of its boundaries. Using the Fourier transform technique, analytical results are obtained for the slip-flow/Navier–Stokes limit. These results are complemented by low-variance simulations of the Boltzmann equation, which are useful for establishing the limits of the slip-flow description, as well as for bridging the gap between the slip-flow analysis and previously developed free-molecular analytical predictions. Results are presented for both periodic (sinusoidal) and nonperiodic (step-jump) heating profiles. Our slip-flow solution is used to elucidate a singular limit reported in the literature for oscillatory heating of a dynamically incompressible fluid. © *2010 American Institute of Physics*. [doi:10.1063/1.3437602]

I. INTRODUCTION

The time response of a fluid confined in a channel and subject to a change in the thermal properties of its boundaries is a classical problem of fundamental importance and broad range of applications; as a result, it has been studied extensively in the context of both classical fluid mechanics[1] and rarefied gas dynamics.[2] The fluid motion induced in this problem is essentially driven by the mechanism of thermal expansion, coupling temperature variations in the fluid with density gradients. Current interest in analyzing unsteady heating processes is motivated by the common occurrence of time-varying boundary temperatures in a wide scope of microelectromechanical and nanoelectromechanical applications, ranging from microprocessor chip heating[3] to ultrafast temperature variations encounted in the laser industry.[4,5] This has resulted in the need to examine this problem in the context of small length scales and short time scales.

The problem of unsteady heating has been studied in the context of continuum gas dynamics in a series of papers[6,7] under the assumption of gradual changes in wall thermal states. To satisfy the continuum assumption, a heating time scale longer than some modest multiple of the molecular collision time has been assumed. To consider shorter time scales, several researchers have investigated the problem in the limit of sudden temperature variations by examining the kinetic response of a dilute gas to a step function change in wall temperatures.[8–12] Close agreement between analytical predictions and molecular simulations has been demonstrated in Ref. 12. A more recent work[13] has focused on the effect of rapidly varying continuous changes in the wall temperatures with characteristic time scales of the order of, or smaller than, the mean collision time, where the effect of molecular collisions is small. Utilizing a collisionless description, closed-form solutions were obtained for the step-jump[12] and high-frequency oscillatory[13] heating problems. In the former, the results obtained describe the early time (not exceeding the molecular collision time) behavior in arbitrarily large systems. In the latter, the hydrodynamic response was found to be confined to thin bounded layers in the vicinity of the walls at all times.

In this work, we complement the above investigations by studying the remaining Knudsen-number regimes of interest, namely, the collision-dominated Navier–Stokes (NS) limit and the transition regime between the NS and the collisionless limits.[14] In the NS limit, the gas behavior is modeled by the viscous-compressible NS equations subject to slip-flow boundary conditions. To first order in the Knudsen number, the latter reduce to impermeability conditions for the normal component of the flow velocity and temperature-jump conditions at the boundaries. This is a commonly used model which has been applied to the study of various problems.[14–17] We solve the resulting set of equations for an arbitrary small-amplitude heating profile using the Fourier transform technique; we focus, in particular, on oscillatory variations and discontinuous step-jump changes. For oscillatory variations, transition from NS to the collisionless regime occurs due to decreasing characteristic length scales or increasing oscillation frequencies. For step changes, the response starts out as collisionless[12] (for short times compared to the collision time), and then transitions to NS-type behavior (for times long compared to the collision time). Transition-regime solutions of the Boltzmann equation are obtained using low-variance Monte Carlo simulations.[18,19]

Our NS results for the oscillatory case are used to reexamine a singular limit reported by Yariv and Brenner[20] for the case of oscillatory heating of a thermally expandable but dynamically incompressible fluid. In their work, Yariv and Brenner[20] concluded that the flow-field becomes two-dimensional in the absence of coupling between density and pressure variations. We find that this conclusion becomes invalid when dynamical compressibility effects are included,

[a)]Present address: Faculty of Aerospace Engineering, Technion—Israel Institute of Technology, Technion City, Haifa 32000, Israel. Electronic mail: avshalom@aerodyne.technion.ac.il.

since the latter leads to a well-posed one-dimensional description.

The paper is organized as follows: in Sec. II, the general linearized problem is described. The problem in the NS/slip-flow limit is formulated and solved in Sec. III, using the Fourier transform technique. Our low-variance simulation method is outlined in Sec. IV. Results for periodic (sinusoidal) and nonperiodic (step-jump) heating profiles are presented and discussed in Secs. V and VI, respectively. Some concluding remarks are given in Sec. VII.

II. PROBLEM DESCRIPTION

Consider a perfect monatomic gas layer of mean density ρ_0 confined between two infinitely long, accommodating walls placed in the (y^*,z^*) plane at $x^*=\pm L/2$ (* denotes a dimensional variable). The walls are heated uniformly with prescribed time dependence and their common temperature is $T_w^*(t^*)=T_0[1+\epsilon F(t^*)]$. It is assumed that the amplitude of the unsteady term is small ($\epsilon \ll 1$), so that the system description may be linearized about its equilibrium state of uniform density ρ_0 and temperature T_0.

We assume a one-dimensional setup where all variables are x^*-dependent and the velocity vector $\mathbf{u}^*$ has a nonzero component only in the x^*-direction. To render the problem dimensionless, we scale the position by the layer width L and the time by a time scale τ^*, characterizing the rate of temperature change at the walls. The velocity is scaled by L/τ^* and the density and temperature are normalized by ρ_0 and T_0, respectively.

We consider both hard-sphere[21] and Bhatnagar, Gross, and Krook[22] (BGK) models of molecular interaction for which efficient low-variance Monte Carlo solution methods exist (see Sec. IV). In the nondimensional formulation, the problem is governed by the Knudsen number, $\mathrm{Kn}=l/L$, where l is the mean free path of a gas molecule, as well as the Strouhal number,[23] $\mathrm{St}=L/(\tau^*\sqrt{RT_0})$, where R is the specific gas constant. As a matter of convenience, we also define the modified Knudsen number, $\widetilde{\mathrm{Kn}}=\mu_0/(\rho_0\sqrt{RT_0}L)$, where μ_0 is the gas dynamic viscosity at reference-equilibrium conditions. The modified Knudsen number is related to Kn through

$$\widetilde{\mathrm{Kn}}=\frac{\mu_0}{\rho_0\sqrt{RT_0}l}\mathrm{Kn}, \tag{2.1}$$

where $\mu_0/(\rho_0\sqrt{RT_0}l)$ is a constant of order unity ($=5\sqrt{2\pi}/16$ for the hard-sphere gas[21] and $=\sqrt{\pi/8}$ for a BGK gas[23]). In addition, we define γ as the ratio of specific heats and use Pr to denote the Prandtl number. For a perfect monatomic gas, $\gamma=5/3$. The Prandtl number takes the values $\mathrm{Pr}=2/3$ for a hard-sphere gas and $\mathrm{Pr}=1$ for the BGK model.

III. SLIP-FLOW LIMIT

In this section, we focus on the case where the distance L between the walls is large compared with the molecular mean free path l (i.e., the Knudsen number $\mathrm{Kn}\ll 1$) and the characteristic time scale of the temperature variations at the boundaries (or the time elapsed from the occurrence of any discontinuous thermal forcing at the walls) is large compared with the mean time between collisions. We model the system evolution using the viscous-compressible NS equations subject to slip-flow boundary conditions.[14] In the present notation, our assumption that the characteristic time scale τ^* is much longer than the mean time between collisions $\tau^*_{\mathrm{coll}}=l/\sqrt{8RT_0/\pi}$, can be expressed as $\mathrm{StKn}\ll\sqrt{8/\pi}\approx 1.6$. We comment on the validity of this condition in Secs. V and VI, where specific examples are considered.

Linearizing about the initial equilibrium state, we obtain the following balances of mass, momentum, and energy for the $O(\epsilon)$ density ρ, normal velocity u, and temperature T perturbations:

$$\frac{\partial\rho}{\partial t}+\frac{\partial u}{\partial x}=0, \tag{3.1}$$

$$\frac{\partial u}{\partial t}=-\frac{1}{\mathrm{St}^2}\left(\frac{\partial\rho}{\partial x}+\frac{\partial T}{\partial x}\right)+\frac{4\widetilde{\mathrm{Kn}}}{3\mathrm{St}}\frac{\partial^2 u}{\partial x^2}, \tag{3.2}$$

and

$$\frac{\partial T}{\partial t}=\frac{\gamma\widetilde{\mathrm{Kn}}}{\mathrm{PrSt}}\frac{\partial^2 T}{\partial x^2}-(\gamma-1)\frac{\partial u}{\partial x}, \tag{3.3}$$

together with the boundary conditions

$$u=0 \quad \text{and} \quad T=F(t)\pm\xi\frac{\partial T}{\partial x} \quad \text{at} \quad x=\mp 1/2. \tag{3.4}$$

The boundary conditions (3.4) impose impermeability and specify the magnitude of temperature jump at the walls. The latter is determined by the value of the temperature gradient at the walls and a temperature-jump coefficient $\xi=\zeta\mathrm{Kn}$, with ζ taking the values $\zeta=2.1269$ for a hard-sphere gas and $\zeta=1.3\sqrt{\pi}/2$ for the BGK model.[23]

We solve for the above problem by introducing the Fourier transform

$$\bar{G}(x,\omega)=\int_{-\infty}^{\infty}G(x,t)\exp[-\mathrm{i}\omega t]\mathrm{d}t \tag{3.5}$$

and applying it to Eqs. (3.1)–(3.4). This yields a system of ordinary equations

$$\mathrm{i}\omega\bar{\rho}+\bar{u}'=0, \tag{3.6}$$

$$\mathrm{i}\omega\bar{u}=-\frac{1}{\mathrm{St}^2}(\bar{\rho}'+\bar{T}')+\frac{4\widetilde{\mathrm{Kn}}}{3\mathrm{St}}\bar{u}'', \tag{3.7}$$

$$\mathrm{i}\omega\bar{T}=\frac{5\widetilde{\mathrm{Kn}}}{3\mathrm{PrSt}}\bar{T}''-\frac{2}{3}\bar{u}', \tag{3.8}$$

where the primes denote differentiations with x, accompanied by the boundary conditions

$$\bar{u}=0 \quad \text{and} \quad \bar{T}=\bar{F}\pm\xi\bar{T}' \quad \text{at} \quad x=\mp 1/2. \tag{3.9}$$

The density and velocity perturbations can be eliminated using

$$\bar{\rho} = \frac{\mathrm{i}}{\omega}\bar{u}',$$

$$\bar{u} = -\frac{5\widetilde{\mathrm{Kn}}}{2\omega \mathrm{PrSt}^2}\left(\frac{1}{\omega \mathrm{St}} + \frac{4\mathrm{i}\widetilde{\mathrm{Kn}}}{3}\right)\bar{T}''' - \frac{1}{\mathrm{St}}\left(2\widetilde{\mathrm{Kn}} - \frac{5\mathrm{i}}{2\omega \mathrm{St}}\right)\bar{T}' \tag{3.10}$$

to yield a single equation for the temperature

$$\frac{5\widetilde{\mathrm{Kn}}}{3\mathrm{PrSt}^2}\left(\frac{4\widetilde{\mathrm{Kn}}}{3} - \frac{\mathrm{i}}{\omega \mathrm{St}}\right)\bar{T}'''' - \frac{1}{3\mathrm{St}}\left(\frac{5}{\mathrm{St}} + 4\mathrm{i}\omega\widetilde{\mathrm{Kn}} + \frac{5\mathrm{i}\omega\widetilde{\mathrm{Kn}}}{\mathrm{Pr}}\right)\bar{T}'' - \omega^2\bar{T} = 0, \tag{3.11}$$

which should be solved in conjunction with the four boundary conditions

$$\frac{5\widetilde{\mathrm{Kn}}}{\mathrm{PrSt}}\left(\frac{1}{\mathrm{St}} + \frac{4\mathrm{i}\omega\widetilde{\mathrm{Kn}}}{3}\right)\bar{T}''' - \left(\frac{5\mathrm{i}\omega}{\mathrm{St}} - 4\omega^2\widetilde{\mathrm{Kn}}\right)\bar{T}' = 0 \quad \text{and}$$

$$\bar{T} = \bar{F} \pm \xi\bar{T}' \quad \text{at} \quad x = \mp 1/2. \tag{3.12}$$

The characteristic polynomial of Eq. (3.11) has four distinct roots

$$r_{1,2}(\omega) = \pm\frac{-a_1 + \sqrt{a_1^2 - 4a_2a_0}}{2a_2} \quad \text{and}$$

$$r_{3,4}(\omega) = \pm\frac{-a_1 - \sqrt{a_1^2 - 4a_2a_0}}{2a_2}, \tag{3.13}$$

where a_0, a_1, and a_2 are the coefficients of $\bar{T}$, $\bar{T}''$, and $\bar{T}''''$ in Eq. (3.11), respectively. The symmetry of the boundary conditions (3.12) implies that $\bar{T}(x) = \bar{T}(-x)$ and therefore

$$\bar{T}(x,\omega) = A(\omega)\cosh[r_1(\omega)x] + B(\omega)\cosh[r_3(\omega)x]. \tag{3.14}$$

Substituting Eq. (3.14) into Eq. (3.12) yields

$$A(\omega) = \left\{-\frac{r_1(c_1r_1^2 - c_2)\sinh(-r_1/2)}{r_3(c_1r_3^2 - c_2)\sinh(-r_3/2)} \times\left[\cosh\left(-\frac{r_3}{2}\right) - \xi r_3\sinh\left(-\frac{r_3}{2}\right)\right] + \cosh\left(-\frac{r_1}{2}\right) - \xi r_1\sinh\left(-\frac{r_1}{2}\right)\right\}^{-1}\bar{F}(\omega),$$

$$B(\omega) = -\frac{r_1(c_1r_1^2 - c_2)\sinh(-r_1/2)}{r_3(c_1r_3^2 - c_2)\sinh(-r_3/2)}A(\omega), \tag{3.15}$$

where

$$c_1 = \frac{5\widetilde{\mathrm{Kn}}}{\mathrm{PrSt}}\left(\frac{1}{\mathrm{St}} + \frac{4\mathrm{i}\omega\widetilde{\mathrm{Kn}}}{3}\right) \quad \text{and} \quad c_2 = \frac{5\mathrm{i}\omega}{\mathrm{St}} - 4\omega^2\widetilde{\mathrm{Kn}}. \tag{3.16}$$

The expressions for the Fourier-transformed density and velocity perturbations now follow from substituting Eq. (3.14) into Eq. (3.10). In addition, the normal heat flux is given by Fourier's law, which in nondimensional representation takes the form

$$\bar{q} = -\frac{5\mathrm{Pr}\widetilde{\mathrm{Kn}}}{2}\bar{T}'. \tag{3.17}$$

The physical solution is obtained by taking the real part of the inverse Fourier transform of each of the transformed hydrodynamic fields

$$G(x,t) = \frac{1}{2\pi}\int_{-\infty}^{\infty}\bar{G}(x,\omega)\exp[\mathrm{i}\omega t]\mathrm{d}\omega. \tag{3.18}$$

This general procedure allows us to obtain analytical or semianalytical results for a variety of problems (heating waveforms) of practical interest. We use this approach in Sec. V to obtain analytical results for the case of sinusoidal heating. In Sec. VI, we obtain semianalytical results for the late-time gas response to step-jump boundary heating. These results are validated and extended by variance-reduced Monte Carlo solutions of the Boltzmann equation. Specifically, in the case of sinusoidal heating, Boltzmann equation solutions are used to bridge the gap between the present slip-flow and previously obtained collisionless-flow results.[13] In the case of step-jump heating, Boltzmann solutions are used to assess the accuracy of the slip-flow description at early times after the jump and describe the transition from our previous free-molecular analysis.[12] The low-variance simulation procedure used here is described in Sec. IV.

IV. NUMERICAL SIMULATIONS

The prevalent numerical scheme for solving the Boltzmann equation is a stochastic particle method known as the direct simulation Monte Carlo (DSMC) method.[24] The linearized ($\epsilon \ll 1$) problem studied here is, however, very difficult to simulate using the DSMC method. This is due to the small hydrodynamic signals associated with the induced hydrodynamic fields, such as the heat-flux and gas-flow velocity. These limitations become particularly severe for $\mathrm{St} \lesssim 10$, where the resolution of the flow velocity using the DSMC method requires massively parallel computing resources.[25] To overcome this difficulty, our numerical solutions are obtained using a recently developed variance-reduced particle method akin to DSMC, known as low-variance deviational simulation Monte Carlo (LVDSMC). By simulating only the *deviation* from equilibrium, this method achieves significant variance reduction, thus reducing the cost associated with low-uncertainty simulation of weak-signal flows or enabling simulations which are intractable using DSMC.

Two variants of the LVDSMC method are applied below to validate the present analysis: the hard-sphere gas is simulated using the scheme described in Homolle and Hadjiconstantinou,[18] and the BGK model is simulated using a particularly efficient method developed by Radtke and Hadjiconstantinou[19] for treating the linearized Boltzmann equation in the relaxation-time approximation. In contrast to DSMC, the low Knudsen numbers considered here do not pose particular problems for the LVDSMC method, as the latter simulates the deviation from a spatially variable equi-

librium and is able to take advantage of the near-local-equilibrium conditions prevalent at low Kn.[19] To eliminate nonlinear effects (in accordance with our linear theoretical model), the hard-sphere calculations were performed with $\epsilon=0.002$; this consideration does not arise in the BGK simulations since the method used solves the linearized Boltzmann equation.

In general, the statistical uncertainty of our simulations depends on the problem parameters (as in the case of low St, which results in very low gas velocities[25]). An upper bound on the statistical uncertainty of all hydrodynamic variables is ≈ 0.004 (in nondimensional units).

V. SINUSOIDAL HEATING

A. Slip-flow solution

The case of sinusoidal heating, $F(t^*)=F_s(t^*)=\sin\omega_p^* t^*$, is amenable to analytical solution. The natural time scale τ^* describing the temperature variations at the walls is associated with the inverse dimensional frequency $\tau^*=1/\omega_p^*$. Consequently, the Strouhal number in this case is defined by $\mathrm{St}=\omega_p^* L/\sqrt{RT_0}$.

To obtain a closed-form solution, we substitute $\bar{F}_s(\omega)=\pi\mathrm{i}[\delta(\omega+1)-\delta(\omega-1)]$, where δ is the Dirac delta function, into Eqs. (3.14)–(3.16) and take the inverse Fourier transform (3.18). This yields an expression for the temperature

$$T(x,t)=[A_s\cosh(r_{s_1}x)+B_s\cosh(r_{s_3}x)]\exp[\mathrm{i}t], \tag{5.1}$$

where, retaining terms $O(\widetilde{\mathrm{Kn}})$, r_{s_1} and r_{s_3} are given by

$$r_{s_1}=\sqrt{\frac{\mathrm{PrSt}}{2\widetilde{\mathrm{Kn}}}}\left[(1+\mathrm{i})+\frac{\widetilde{\mathrm{Kn}}\mathrm{St}}{5}(-1+\mathrm{i})\left(\frac{1}{\mathrm{Pr}}-\frac{4}{3}\right)\right]+O(\widetilde{\mathrm{Kn}^2}) \tag{5.2}$$

and

$$r_{s_3}=\sqrt{\frac{3}{5}}\mathrm{St}\left(\mathrm{i}+\frac{2}{3}\widetilde{\mathrm{Kn}}\mathrm{St}\right)+O(\widetilde{\mathrm{Kn}^2}). \tag{5.3}$$

In addition,

$$A_s=-\mathrm{i}\left\{-\frac{r_{s_1}(c_{s_1}r_{s_1}^2-c_{s_2})\sinh(-r_{s_1}/2)}{r_{s_3}(c_{s_1}r_{s_3}^2-c_{s_2})\sinh(-r_{s_3}/2)}\times\left[\cosh\left(-\frac{r_{s_3}}{2}\right)-\xi r_{s_3}\sinh\left(-\frac{r_{s_3}}{2}\right)\right]+\cosh\left(-\frac{r_{s_1}}{2}\right)-\xi r_1\sinh\left(-\frac{r_{s_1}}{2}\right)\right\}^{-1}\quad\text{and}$$

$$B_s=-\frac{r_{s_1}(c_{s_1}r_{s_1}^2-c_{s_2})\sinh(-r_{s_1}/2)}{r_{s_3}(c_{s_1}r_{s_3}^2-c_{s_2})\sinh(-r_{s_3}/2)}A_s, \tag{5.4}$$

with

$$c_{s_1}=\frac{5\widetilde{\mathrm{Kn}}}{\mathrm{PrSt}}\left(\frac{4\widetilde{\mathrm{Kn}}}{3}-\frac{\mathrm{i}}{\mathrm{St}}\right)\quad\text{and}\quad c_{s_2}=\frac{5}{\mathrm{St}}+4\mathrm{i}\widetilde{\mathrm{Kn}}. \tag{5.5}$$

The expressions for the density, velocity, and heat-flux perturbations follow from Eqs. (3.10) and (3.17) to be

$$\rho(x,t)=\left[-\frac{5\mathrm{i}\widetilde{\mathrm{Kn}}}{2\mathrm{PrSt}^2}\left(\frac{1}{\mathrm{St}}+\frac{4\mathrm{i}\widetilde{\mathrm{Kn}}}{3}\right)[A_s r_{s_1}^4\cosh(r_{s_1}x)+B_s r_{s_3}^4\cosh(r_{s_3}x)]-\frac{\mathrm{i}}{\mathrm{St}}\left(2\widetilde{\mathrm{Kn}}-\frac{5\mathrm{i}}{2\mathrm{St}}\right)\times[A_s r_{s_1}^2\cosh(r_{s_1}x)+B_s r_{s_3}^2\cosh(r_{s_3}x)]\right]\exp[\mathrm{i}t], \tag{5.6}$$

$$u(x,t)=\left[-\frac{5\widetilde{\mathrm{Kn}}}{2\mathrm{PrSt}^2}\left(\frac{1}{\mathrm{St}}+\frac{4\mathrm{i}\widetilde{\mathrm{Kn}}}{3}\right)[A_s r_{s_1}^3\sinh(r_{s_1}x)+B_s r_{s_3}^3\sinh(r_{s_3}x)]-\frac{1}{\mathrm{St}}\left(2\widetilde{\mathrm{Kn}}-\frac{5\mathrm{i}}{2\mathrm{St}}\right)\times[A_s r_{s_1}\sinh(r_{s_1}x)+B_s r_{s_3}\sinh(r_{s_3}x)]\right]\exp[\mathrm{i}t], \tag{5.7}$$

and

$$q(x,t)=-\frac{5\mathrm{Pr}\widetilde{\mathrm{Kn}}}{2}[A_s r_{s_1}\sinh(r_{s_1}x)+B_s r_{s_3}\sinh(r_{s_3}x)]\exp[\mathrm{i}t]. \tag{5.8}$$

The physical fields are obtained by taking the real parts of Eqs. (5.1) and (5.6)–(5.8).

B. The case St$\sim O(1)$

Figure 1 presents the space variations in the density, temperature, velocity, and heat-flux perturbations for a BGK gas subject to sinusoidal heating at Kn=0.025 and $\mathrm{St}=\pi\sqrt{2}/4\approx 1.11$ at the indicated times in $\tau_p=2\pi$ period-time units. The solid lines mark the analytical expressions (5.1) and (5.6)–(5.8) and the crosses denote LVDSMC data. Figure 2 shows the space variations in the velocity and temperature fluctuations for a hard-sphere gas at the same parameter combination. Good agreement is observed between analysis and LVDSMC results.

Close inspection of the hydrodynamic fields reveals the presence of thin Knudsen layers in the vicinity of the walls, leading to small discrepancies ($\approx 2\%$) between the Boltzmann result and the NS solution [see the inset in Fig. 2(b)]. However, at Kn=0.025, these effects are small and the slip-flow solution captures the temperature jump at the walls satisfactorily [see the circles in Figs. 1(b) and 2(b) and Fig. 1 caption]. Note that among the hydrodynamic fields presented, the velocity is typically much smaller than the others.

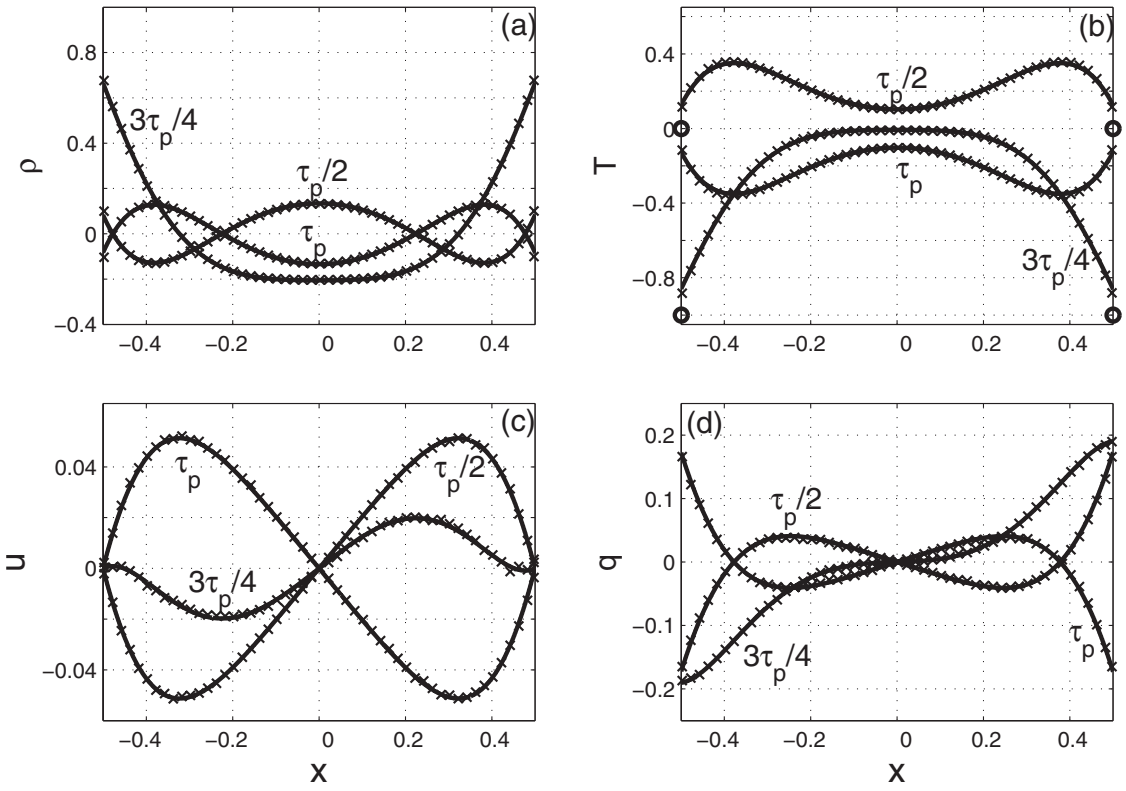

FIG. 1. The (a) density, (b) temperature, (c) velocity, and (d) heat-flux perturbations for a BGK gas subject to sinusoidal heating at Kn=0.025, St= $\pi\sqrt{2}/4 \approx 1.11$, and times $t=\tau_p/2$, $t=3\tau_p/4$, and $t=\tau_p$, where $\tau_p=2\pi$ is the period time. The solid lines correspond to expressions (5.1) and (5.5)–(5.7), and the crosses mark LVDSMC data. The circles in (b) denote the corresponding wall-temperature perturbations, and are useful for visualizing the temperature jump at the walls.

In the hard-sphere case (which is more expensive to simulate), this weak velocity signal results in perceptible statistical noise [see Fig. 2(a)]. With decreasing St, both density and heat flux follow this behavior and become considerably smaller than the temperature (see Sec. V C).

To examine the limits of the slip-flow solution at higher values of Kn and St, Figs. 3 and 4 show comparisons between NS theory and Boltzmann simulation for the velocity and temperature perturbations for a BGK gas; Fig. 3 provides a comparison for increasing Kn at a constant St= $\pi\sqrt{2}/4 \approx 1.11$, while Fig. 4 features a comparison for increasing St at a constant Kn=0.025.

Starting with Fig. 3, we observe that at the lowest Knudsen presented (Kn=0.05), the agreement between the results is very good, apart from small Knudsen-layer discrepancies in the temperature profile near the walls. At Kn=0.1, the overall agreement is still satisfactory, but a small systematic difference ($\lesssim 5\%$) in the temperature is observed throughout the domain. As expected, at the largest Knudsen number presented, namely, Kn=0.2, kinetic effects become important and the NS solution provides only a qualitative description. We comment further on the behavior of the solution at larger Knudsen numbers in Sec. V E.

Figure 4 presents results for constant Kn=0.025 and varying St/($\pi\sqrt{2}$)=2, 4, and 8, corresponding to StKn ≈ 0.22, 0.44, and 0.89, respectively. Recall that StKn $\ll \sqrt{8/\pi} \approx 1.6$ is required for the mean free time to be much smaller than the characteristic time ω_p^{*-1}. At the lowest StKn presented (≈ 0.22), the agreement between analysis and simulation is good and discrepancies are limited to the near-wall regions. With increasing StKn, the hydrodynamic perturbations become confined to the neighborhood of the boundaries; at the same time, the differences between NS theory and simulation increase, as observed in the temperature profile for St/($\pi\sqrt{2}$)=8. This trend continues with further increasing St; this is further discussed in Sec. V D, where we describe the transition to the bounded-layer solution in the limit St $\gg 1$.[13]

C. The case St $\ll 1$

Yariv and Brenner[20] have considered the oscillatory heating problem for a fluid and studied the "weak thermal forcing limit," where density variations result only from thermal expansion. In other words, the effects of dynamic compressibility, coupling density and pressure variations, were ignored. Consequently, the density perturbation is governed entirely by the temperature which can replace it in the continuity equation (3.1). The mass and energy balances, Eqs. (3.1) and (3.3), are then decoupled from the momentum equation (3.2). After solving for the temperature in Eq. (3.3), the continuity equation (3.1) yields a first-order equation for the velocity; its solution, however, cannot satisfy impermeability conditions at both walls. Yariv and Brenner[20] have therefore concluded that the flow-field must be two-dimensional.

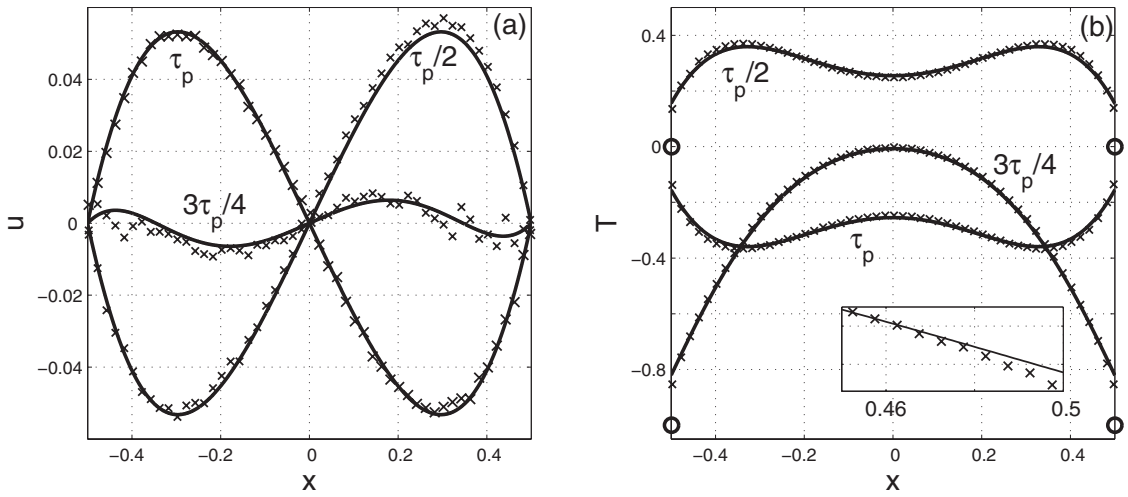

FIG. 2. The (a) velocity and (b) temperature perturbations for a hard-sphere gas subject to sinusoidal heating at Kn=0.025, St=$\pi\sqrt{2}/4\approx 1.11$, and the indicated values of time. All notations as in Fig. 1. The inset in (b) is a magnification of the lower right end of the $t=3\tau_p/4$ curve, where a thin Knudsen layer is observed.

We suggest here a different line of thought by allowing for small (but finite) dynamic compressibility in the fluid. It is our contention that, to some extent, such an assumption is always valid for a gas. We focus on the case where $\mathrm{St}\ll\widetilde{\mathrm{Kn}}$ and define the Reynolds number

$$\mathrm{Re}\equiv\frac{\mathrm{St}}{\widetilde{\mathrm{Kn}}}=\frac{\rho_0\omega_p^* L^2}{\mu_0}\ll 1.$$

Assuming harmonic time dependence of the solution, we introduce the asymptotic expansion

$$G(x,t)=\{G^{(0)}(x)+\mathrm{Re}[G^{(1)}(x)+\widetilde{\mathrm{Kn}}G^{(2)}(x)+\widetilde{\mathrm{Kn}}^2G^{(3)}(x)+\ldots]\}\exp[it] \tag{5.9}$$

for each of the hydrodynamic perturbations $G\in\{\rho,u,T,q\}$. Substituting Eq. (5.9) into Eqs. (3.1)–(3.3) yields for the leading terms

$$T^{(0)}=-\mathrm{i}\quad\text{and}\quad\rho^{(0)}=u^{(0)}=0, \tag{5.10}$$

in accordance with the leading order of the boundary conditions (3.4) for the temperature. Next, the leading $O(1)$ of the energy equation (3.3) yields a balance between convection and conduction terms. This determines the $O(\mathrm{Re})$ correction for the temperature

$$T^{(1)}(x)=\frac{3\mathrm{Pr}}{10}\left(x^2-\frac{1}{4}\right), \tag{5.11}$$

which satisfies the corresponding $O(\mathrm{Re})$ homogeneous boundary conditions.

The difference from the analysis of Yariv and Brenner[20] can be visualized by considering the leading balance $O(1/\widetilde{\mathrm{StKn}})$ of the momentum equation (3.2), relating the space variations in the density and temperature. An integration with x yields

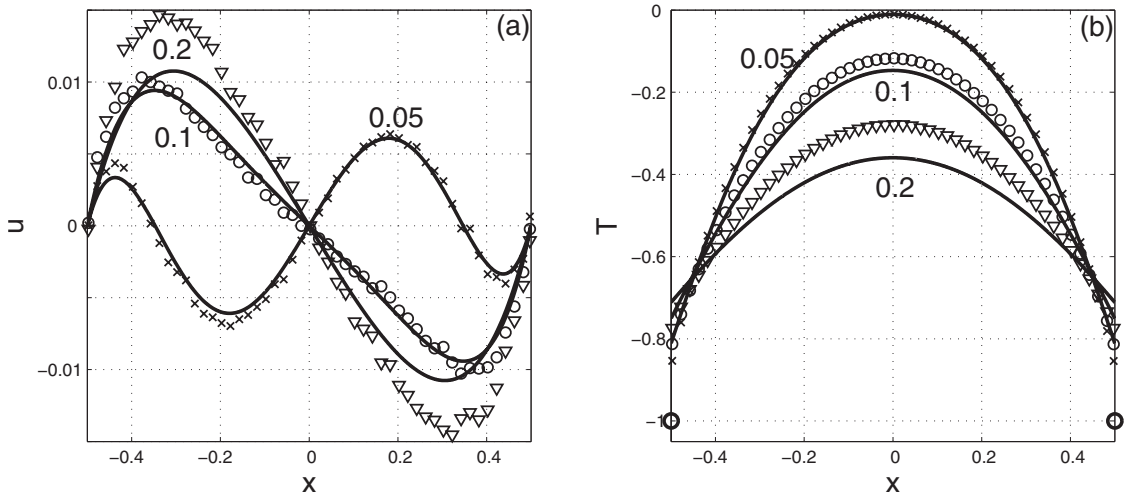

FIG. 3. The (a) velocity and (b) temperature perturbations for a BGK gas subject to sinusoidal heating at $t=3\tau_p/4=3\pi/2$, St=$\pi\sqrt{2}/4\approx 1.11$, and the indicated values of Kn. The solid lines correspond to the analytical solution and the symbols mark LVDSMC data. The circles at $(-0.5,-1)$ and $(0.5,-1)$ denote the wall-temperature perturbations.

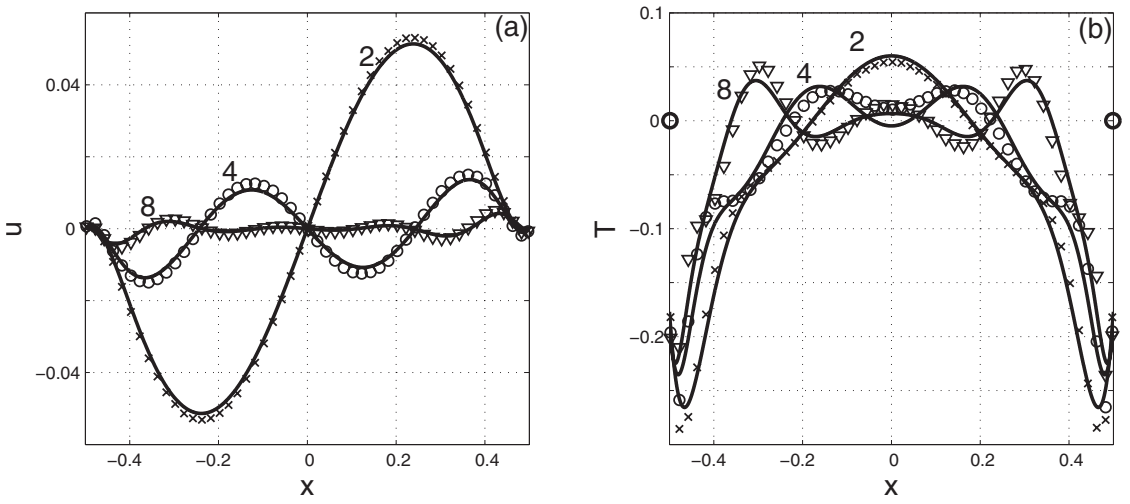

FIG. 4. The (a) velocity and (b) temperature perturbations for a BGK gas subject to sinusoidal heating at $t=\tau_p=2\pi$, Kn=0.025, and the indicated values of $\mathrm{St}/(\pi\sqrt{2})$. The solid lines correspond to the analytical solution and the symbols mark LVDSMC data. The circles at (−0.5, 0) and (0.5,0) in (b) denote the wall-temperature perturbations.

$$\rho^{(1)}(x) = -T^{(1)}(x) + K_1. \tag{5.12}$$

It is the introduction of $K_1 \neq 0$ that decouples the time variations in the density and temperature, thus allowing for the effect of dynamic compressibility [cf. Eq. (2) in Ref. 20]. Substituting Eq. (5.12) (multiplied by $\exp[\mathrm{i}t]$) into Eq. (3.1) and integrating with x yields the leading-order expression for the velocity

$$u^{(1)}(x) = \mathrm{i}\int^{x} T^{(1)}(\tilde{x})\mathrm{d}\tilde{x} - \mathrm{i}K_1 x + K_2. \tag{5.13}$$

In contrast to Ref. 20, the two constants of integration appearing in Eq. (5.13), namely, K_1 and K_2, enable this solution to satisfy the impermeability condition, Eq. (3.4), at *both* walls. Calculating K_1 and K_2 and obtaining the heat flux from the time-counterpart of Eq. (3.17), we find the leading-order approximation[26]

$$\begin{aligned} T &= \left[-\mathrm{i} + \frac{3\mathrm{Pr}}{10}\mathrm{Re}\left(x^2 - \frac{1}{4}\right) + O(\mathrm{St})\right]\exp[\mathrm{i}t], \\ \rho &= \left[\frac{\mathrm{Pr}}{10}\mathrm{Re}\left(-3x^2 + \frac{1}{4}\right) + O(\mathrm{St})\right]\exp[\mathrm{i}t], \\ u &= \left[\frac{\mathrm{iPr}}{10}\mathrm{Re}\, x\left(x^2 - \frac{1}{4}\right) + O(\mathrm{St})\right]\exp[\mathrm{i}t], \\ q &= \left[-\frac{3\mathrm{Pr}^2}{2}\mathrm{St}\, x + O(\widetilde{\mathrm{StKn}})\right]\exp[\mathrm{i}t]. \end{aligned} \tag{5.14}$$

The low-Strouhal heat-flow mechanism can now be fully rationalized. The uniform leading-order temperature field equation (5.10) corresponds to the "incompressible" limit where temperature changes at the walls are transmitted instantaneously across the gap. This transmission is enabled through heat conduction [manifested by the leading order of the energy balance equation (3.3)], coupling $O(\mathrm{Re})$ quadratic nonuniformity of the temperature (5.11). This nonuniformity is balanced by the density variations (5.12) in the leading order of the momentum equation (3.2) which, in turn, give rise to the one-dimensional velocity field (5.13) in accordance with the continuity equation (3.1). Recalling that all perturbations are $O(\epsilon)=O(\Delta T/T_0)$, we conclude that the velocity obtained in this case is typically $O(\epsilon\mathrm{Re})$. In essence, it is the decoupling between the time variations in the density and temperature perturbations (arising from the leading order of the momentum equation) that results in the occurrence of one-dimensional (rather than two-dimensional) flow.

D. The case St≫1

The limit of rapid oscillatory heating has been studied by Manela and Hadjiconstantinou[13] for a collisionless gas, where $\mathrm{St}\gg 1$ and $\mathrm{StKn}\gg\sqrt{8/\pi}$. This work has revealed that any nontrivial behavior of the system is confined to thin bounded layers in the vicinity of the boundaries. Here we consider the counterpart problem in the continuum limit, namely, $\mathrm{St}\gg 1$ with $\mathrm{StKn}\ll\sqrt{8/\pi}$. These conditions suggest that as St increases, the slip-flow solution will be valid at smaller Knudsen numbers. In other words, for a sufficiently high St, the slip-flow solution will become invalid at Knudsen numbers significantly lower than the traditionally accepted slip-flow limit of Kn=0.1.[23]

Figure 5 shows the temperature perturbation for a BGK gas subject to high-frequency sinusoidal heating at $\mathrm{St}=40\pi\sqrt{2}$ and various Knudsen numbers. Figure 5(a) focuses on the lower Knudsen number values Kn=0.001 and 0.01, while Fig. 5(b) presents results for Kn=0.1 and 1. In this series of ascending Kn, the product StKn obtains the values ≈0.18, 1.8, 18.8, and 188, respectively. The required condition $\mathrm{StKn}\ll 1.6$ is therefore violated already at Kn=0.01; it is thereby expected that the slip-flow description will only be valid at Kn=0.001. This prediction is confirmed by the results of Fig. 5, which show that while the agreement is very good for Kn=0.001, significant discrepancies are observed at Kn=0.01. These discrepancies are accompanied by

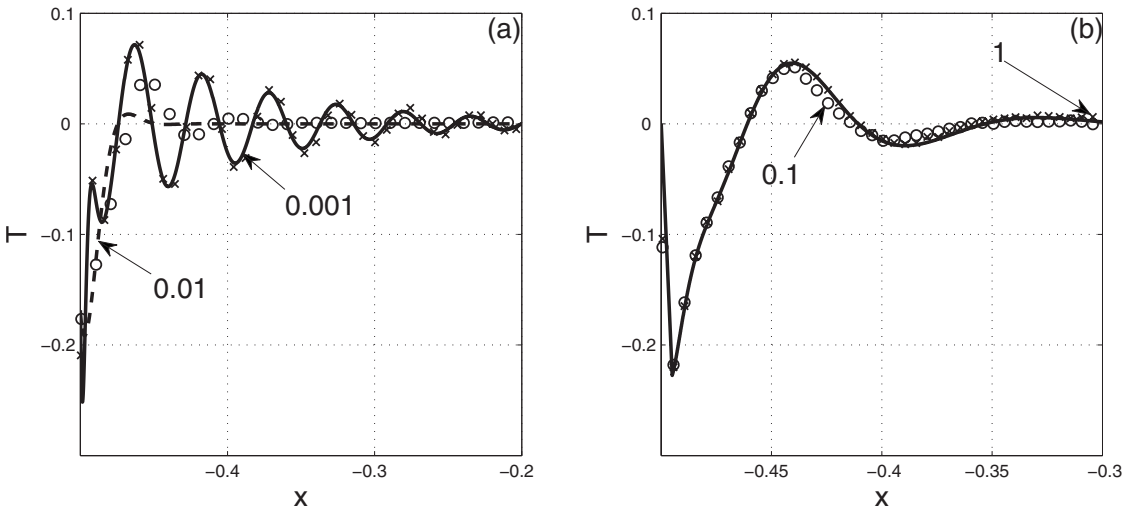

FIG. 5. The temperature perturbation for a BGK gas subject to sinusoidal heating at $t=\tau_p=2\pi$, $\mathrm{St}=40\pi\sqrt{2}$, and (a) Kn=0.001, 0.01, (b) Kn=0.1, 1. In (a), the solid and dashed lines show the slip-flow solution (5.1) at Kn=0.001 and Kn=0.01, respectively; the crosses and circles depict the corresponding LVDSMC data at Kn=0.001 and Kn=0.01. In (b), the solid line marks the high-frequency collisionless approximation obtained in Ref. 13. The circles and crosses mark LVDSMC data at Kn=0.1 and Kn=1, respectively.

the formation of a bounded layer. The transition to the bounded-layer free-molecular solution[13] is completed in Fig. 5(b), where the solid line marks the high-frequency analytical approximation [Eq. (37) in Ref. 13] and the symbols denote the Kn=0.1 (circles) and Kn=1 (crosses) LVDSMC results. At Kn=0.1, the agreement between the collisionless analysis and simulation is already good, with a small "oscillating" error. At Kn=1, the asymptotic result coincides completely with the numerical solution, marking the establishment of the free-molecular regime at a Knudsen number significantly lower than the commonly accepted value of Kn=10.[23]

E. Transition regime

Figure 6 presents a schematic mapping of the different flow regimes obtained in the sinusoidal heating problem in the (Kn,St) plane. The dark-shaded and bright-shaded zones mark the domains of slip-flow and free-molecular regimes, respectively, while the unshaded zone corresponds to the transition domain of "intermediate" Knudsen numbers.

When $\mathrm{St}\lesssim 1$, the characteristic time scale of temperature variations at the boundaries is always considerably larger than the mean collision time. As a result, the limit of validity of our NS results is determined only by the Knudsen number. In this case, our comparison with LVDSMC results confirms the commonly accepted value of $\mathrm{Kn}\approx 0.1$ to be the upper limit of applicability of the slip-flow model (see Fig. 3). The transition regime then extends up to $\mathrm{Kn}\approx 7$ (see Fig. 7), where the effect of molecular collisions vanishes and the free-molecular description, analyzed in Ref. 13, prevails.

The situation changes markedly in the case of high-frequency heating $\mathrm{St}\gg 1$. Here, the short time scale of temperature variations at the walls becomes the main factor in determining the type of flow to be developed; specifically, the StKn criterion replaces the Knudsen number condition used in the $\mathrm{St}\lesssim 1$ case. At $\mathrm{StKn}=\sqrt{8/\pi}$ (denoted by a line passing in the transition zone in Fig. 6), the characteristic time scale $\tau=1/\omega_p$ and the mean collision time τ_{coll} are equal; the slip-flow and collisionless-flow regimes are expected to take place at $\mathrm{StKn}\ll\sqrt{8/\pi}$ and $\mathrm{StKn}\gg\sqrt{8/\pi}$, respectively. In practice, our comparison with LVDSMC data indicates that the transition regime is bounded between $0.2\lesssim\mathrm{StKn}\lesssim 20$ (see Figs. 5 and 7).

To further illustrate the transition between the different flow regimes, Fig. 7 presents the wall normal heat flux, $q_w=q(x=-0.5)$, of a BGK gas subject to sinusoidal heating at different values of St. The figure shows the Kn dependence of the heat-flux amplitude $|q_w|$ [Fig. 7(a)] and normalized phase shift $\phi_{q_w}/2\pi$ [Fig. 7(b)] for $\mathrm{St}/(\pi\sqrt{2})=0.1$, 0.25, 8, and 40, based on the definition

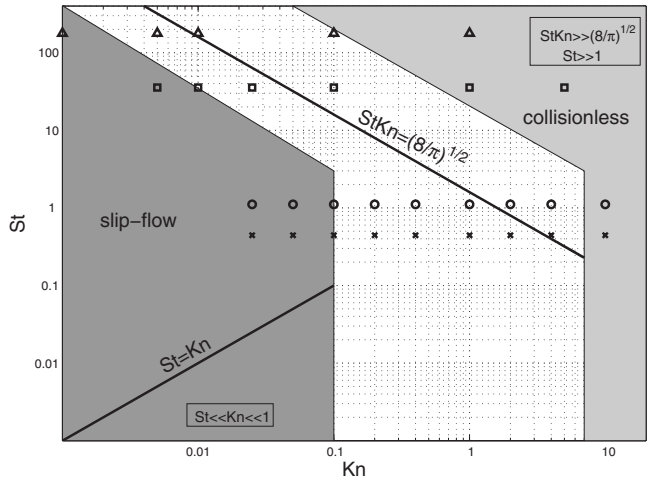

FIG. 6. Schematic partition of the (Kn,St) plane to the different flow domains in the sinusoidal heating problem. The dark-shaded and bright-shaded zones mark the domains of slip-flow and collisionless-flow regimes, respectively. The line $\mathrm{StKn}=\sqrt{8/\pi}$ corresponds to the locus of states, where the characteristic time scale $\tau=1/\omega_p$ is equal to the mean collision time τ_{coll}. The limit cases $\mathrm{St}\ll\mathrm{Kn}\ll 1$ (of small dynamical compressibility) and $\mathrm{StKn}\gg\sqrt{8/\pi}, \mathrm{St}\gg 1$ (of thin bounded layers) are discussed in Secs. V C and V D, respectively. The crosses, circles, squares, and triangles mark the (St,Kn) combinations for which LVDSMC data is presented in Fig. 7.

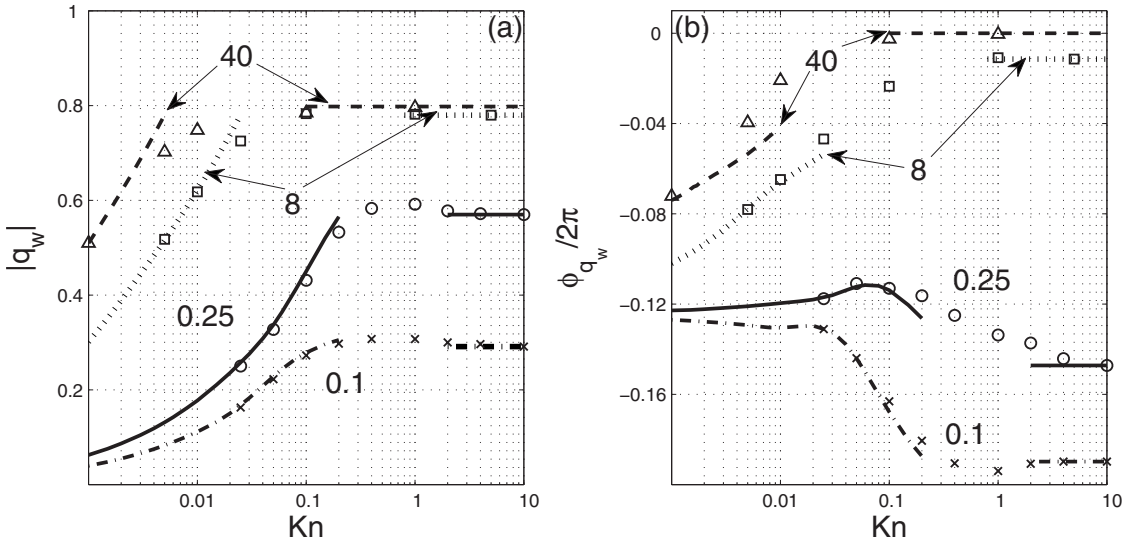

FIG. 7. The Knudsen-number variation in the wall heat-flux (a) amplitude and (b) phase at the indicated values of $\mathrm{St}/(\pi\sqrt{2})$ for a BGK gas subject to sinusoidal heating. The lines mark the analytical slip-flow and collisionless solutions and the symbols denote LVDSMC data.

$$q_w = |q_w|\sin(t - \phi_{q_w}). \tag{5.15}$$

The figure shows that the heat-flux magnitude increases with both St and Kn. For any given St, $|q_w|$ increases at low Kn according to the prediction of our slip-flow theory. When the value of Kn exceeds its slip-flow limit (and enters the transition domain marked by the unshaded zone in Fig. 6), the agreement between theory and LVDSMC calculations breaks down. With further increasing Kn, the effect of molecular collisions diminishes until, at large enough values, the free-molecular regime is established and the heat-flux amplitude attains its collisionless value as obtained in Ref. 13. In the high-frequency limit (illustrated by the $\mathrm{St}=40\pi\sqrt{2}$ case) this value coincides with its asymptotic approximation, $|q_w| \approx \sqrt{2/\pi}$ [note the difference from Eq. (39) in Ref. 13 owing to the different scaling].

Similar characteristics are observed for the behavior of the phase shift in Fig. 7(b). However, the phase-shift approach toward its free-molecular value is not always monotonic and local maxima and minima are observed in some cases. As in Fig. 7(a), for high-frequency ($\mathrm{St}=40\pi\sqrt{2}$) and for sufficiently large Knudsen numbers ($\mathrm{Kn} \gtrsim 0.1$), the high-frequency free-molecular limit [$\phi_{q_w}=0$, see Eq. (39) in Ref. 13] is captured.

VI. STEP-JUMP HEATING

In this section, we study the gas response to step-jump boundary heating, in which the temperature of both boundaries is perturbed instantaneously at $t=0$ from $T_w^*=T_0$ to $T_w^*=T_0(1+\epsilon)$. In nondimensional formulation, the heating signal is given by $F(t)=F_j(t)=\mathrm{H}(t)$, where H is the Heaviside step function. The problem has been investigated in several works, including DSMC simulation studies[11] and theoretical analyses concentrating on the free-molecular limit.[8–10,12] The latter supplies the early time response (for times not exceeding the mean collision time) of arbitrarily large systems. Sone[8] also addressed the near-continuum (late time) limit by considering the problem for a semi-infinite gas expanse using a linearized BGK model; his work has focused on the behavior of the gas in the vicinity of the boundary. In what follows, we aim to complement the above studies by focusing on the late-time system response in a small-scale channel. Our slip-flow solution is expected to be valid in systems characterized by $\mathrm{Kn} \ll 1$ after a sufficiently long time; the latter consideration is further discussed below.

In this problem, we scale the velocity by the mean thermal speed $U_{\mathrm{th}}=\sqrt{2RT_0}$. Consequently, the normalizing time scale is $\tau^*=L/U_{\mathrm{th}}$ and the Strouhal number becomes a constant, $\mathrm{St}=L/\tau^*\sqrt{RT_0}=\sqrt{2}$. The problem is, therefore, governed, apart from the model of molecular interaction, by a single parameter, the Knudsen number. The results are obtained by calculating the inverse transform of the Fourier-transformed hydrodynamic fields, as described in Sec. III.

The Fourier transform of the heating signal in the step-jump problem is

$$\bar{F}_j(\omega) = \int_{-\infty}^{\infty} \mathrm{H}(t)\exp[-\mathrm{i}\omega t]\mathrm{d}t = \pi\delta(\omega) - \mathrm{i}/\omega. \tag{6.1}$$

Substituting $\bar{F}(\omega)=\bar{F}_j(\omega)$ into Eq. (3.15) and then to Eq. (3.14), and carrying out the inverse Fourier transform (3.18), yields

$$T(x,t) = \frac{1}{2} - \frac{\mathrm{i}}{2\pi}\int_{-\infty}^{\infty} \frac{\bar{T}(x,\omega)}{\omega\bar{F}_j(\omega)}\exp[\mathrm{i}\omega t]\mathrm{d}\omega, \tag{6.2}$$

where the two terms on the right-hand side are obtained, respectively, from integration over the delta-function and the inverse-omega terms in Eq. (6.1). The actual calculation of the latter requires numerical integration. The density, velocity, and normal heat-flux perturbations are obtained in a similar manner from Eqs. (3.10), (3.17), and (3.18).

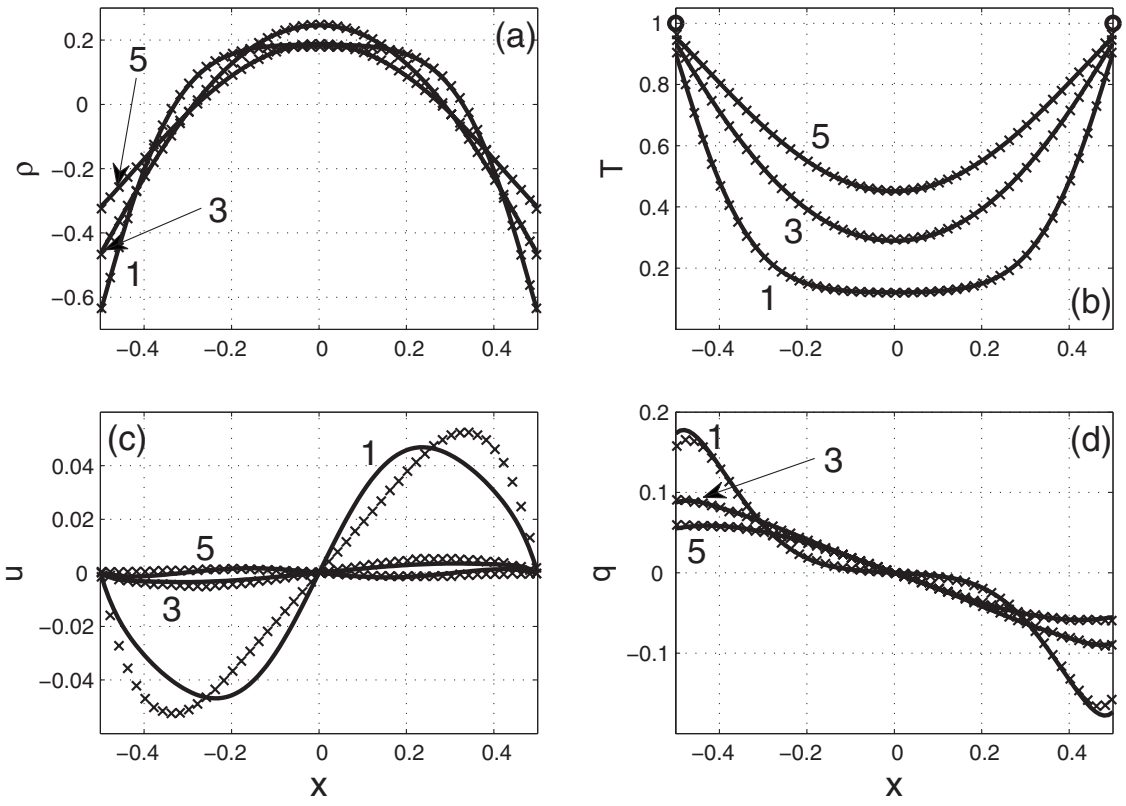

FIG. 8. The (a) density, (b) temperature, (c) velocity, and (d) heat-flux perturbations for a BGK gas subject to step-jump heating at Kn=0.025 and the indicated times. The solid lines correspond to the Fourier transform results and the crosses mark LVDSMC data. The circles denote the wall-temperature perturbations.

It is expected that our analysis will be valid at times much larger than the mean collision time τ_{coll}, after the occurrence of input discontinuity at $t=0$. Recall that according to the original definition of the Strouhal number $\text{St}=L/\tau^*\sqrt{RT_0}$, it is inversely proportional to the characteristic time scale τ^* of temperature variations at the walls. When wall-temperature discontinuities occur, this local time scale becomes vanishingly small, making the corresponding Strouhal number infinitely large. In terms of the present Fourier analysis, such discontinuities can be correctly captured only if infinitely large frequency components are taken into account. As a result, the condition $\text{StKn} \ll \sqrt{8/\pi}$ is inevitably violated and the full kinetic model of the gas must be taken into account. Conversely, for the present slip-flow scheme to be valid, it is required that the contributions of high-frequency terms be small. This can only be ensured when sufficient time ($t \gg \tau_{\text{coll}}$) has elapsed from the moment of discontinuity. In such a case, the infinite domain of integration in Eq. (6.2) may be replaced by a finite range of frequencies over which the NS results of Sec. III are valid.

Figure 8 presents the response of a BGK gas at Kn=0.025 to step-jump heating at its boundaries. The nondimensional value of the mean collision time in this case is $\tau_{\text{coll}}=\sqrt{\pi}/80 \approx 0.022$ (in L/U_{th} time units). In accordance with the above requirement for $t \gg \tau_{\text{coll}}$, the results are presented at times $t=1$, 3, and 5, illustrating the system evolution: the instantaneously heated walls induce lower-density zones in their vicinity which, in turn, generate waves propagating across the channel. With increasing time, the amplitude of these waves decays while the temperature increases monotonically. At late times, the gas acquires its new equilibrium state at the final wall temperature.

The agreement between the present theory and LVDSMC data is very good at almost all times. The most visible exception is the velocity profile at the earliest time $t=1$. As explained above, this discrepancy results from the non-negligible effect of high-frequency components, which cannot be captured correctly by the present theory. Note that the small amplitude of the velocity and the time derivative involved in obtaining it from the density field [see Eq. (3.1)] are the reasons for observing the differences mainly in the velocity. These discrepancies vanish with increasing time, and the late-time gas behavior is fully captured. At times earlier than $t=1$ (not presented here), significant disagreements are observed in all hydrodynamic fields.

To gain further insight into the time evolution of the system, Fig. 9 shows the time dependence of the velocity and temperature perturbations at two locations, namely, $x=-0.4875$ (in the vicinity of the left wall, $x=-0.5$) and $x=-0.3025$, and same conditions as in Fig. 8. The figure compares our LVDSMC data with the present slip-flow theory (for $t \gg \tau_{\text{coll}}$) and previously obtained[12] collisionless analysis (for $t \ll \tau_{\text{coll}}$). For completeness, the latter early time estimates are repeated here

$$u(x,t \ll \tau_{\text{coll}}) \approx \frac{1}{2\sqrt{\pi}}[c_{x_+}^2 \exp(-c_{x_+}^2) - c_{x_-}^2 \exp(-c_{x_-}^2)] \tag{6.3}$$

and

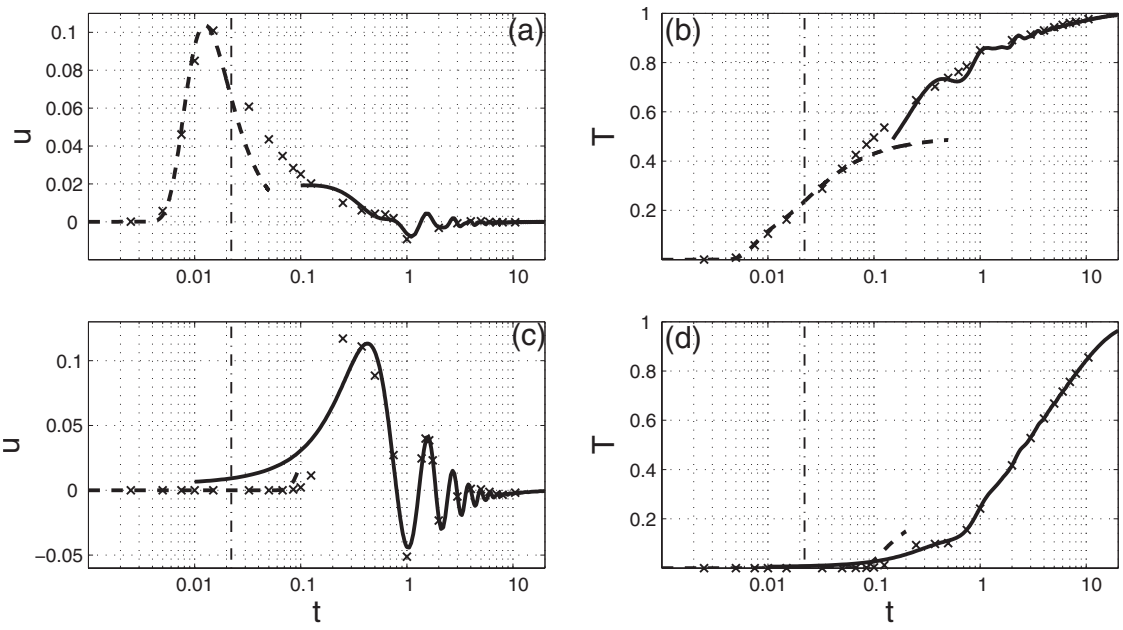

FIG. 9. Time evolution of the [(a) and (c)] velocity and [(b) and (d)] temperature perturbations at [(a) and (b)] $x=-0.4875$ and [(c) and (d)] $x=-0.3025$ for a BGK gas subject to step-jump heating at Kn=0.025. The solid lines correspond to the slip-flow solution (valid for $t \gg \tau_{\mathrm{coll}}$), the dashed lines mark the collisionless result (valid for $t \ll \tau_{\mathrm{coll}}$), and the crosses depict LVDSMC data. The dashed-dotted lines mark the mean collision time $\tau_{\mathrm{coll}}=\sqrt{\pi}/80 \approx 0.022$.

$$T(x,t \ll \tau_{\mathrm{coll}}) \approx \frac{1}{3\sqrt{\pi}}\left\{ c_{x_+}^3 \exp(-c_{x_+}^2) - c_{x_-}^3 \exp(-c_{x_-}^2) + \frac{3\sqrt{\pi}}{2}[\gamma(c_{x_+}) + \gamma(-c_{x_-})]\right\}, \tag{6.4}$$

where $c_{x_\pm}=(x \pm 1/2)/t$ and $\gamma(z)=(2/\sqrt{\pi})\int_z^\infty \exp[-p^2]\mathrm{d}p$ is the complementary error function.

Recalling that our slip-flow analysis should be valid for $t \gg \tau_{\mathrm{coll}} \approx 0.022$, the agreement between the solid lines and LVDSMC data for $t \gtrsim 1$ (i.e., after $\approx$50 collision times) is in place. At early times $t \lesssim \tau_{\mathrm{coll}}$, our previously obtained collisionless results capture the system behavior. This is particularly significant at x-locations close to the wall (such as $x=-0.4875$, which is less than one mean free path away from the boundary for the present Kn=0.025), where the initial nontrivial gas behavior is ballistic. Between these two limits (i.e., at times $\tau_{\mathrm{coll}} \lesssim t \lesssim 50\tau_{\mathrm{coll}}$), the dynamics of the system is governed by the solution of the complete (linearized) Boltzmann equation.

VII. CONCLUSION

We have studied the linearized response of a gas confined in a channel to an arbitrary variation in the temperature of its boundaries. Our results complement existing analyses of the collisionless gas response to high-frequency ($\mathrm{St} \gg 1$) and step-jump heating. The solution obtained is also used to analyze the system response to sinusoidal heating in the limit $\mathrm{St} \ll 1$ (slow heating). In that case, the present analysis elucidates the singular nature of the dynamically incompressible investigation carried out by Yariv and Brenner,[20] by showing that any finite dynamic compressibility effects allow the flow to be one-dimensional. The present scheme provides an accurate and simple description of the gas response in the low-St number limit where numerical calculations are particularly demanding, due to long evolution time scales and small hydrodynamic response amplitudes.

Our results can be extended in several directions. While the present analysis has focused on a BGK and hard-sphere models of molecular interaction, the results can be easily extended to include other models of molecular interaction. Such analyses will essentially modify the numerical values relating Kn and $\widetilde{\mathrm{Kn}}$ in Eq. (2.1) and the magnitude of the temperature-jump coefficient ζ appearing in the boundary conditions [see Eq. (3.4) *et seq.*]. It is also desirable to extend the present scheme to the transition regime of moderate $\mathrm{Kn} \sim O(1)$ numbers and intermediate $t \gtrsim O(\tau_{\mathrm{coll}})$ times. Such analysis may help, for example, in characterizing the heat-flow mechanism in the transition regime of moderate oscillatory heating frequencies (depicted by the unshaded domain of Fig. 6) or in bridging the gap between the early and late-time responses to instantaneous (discontinuous) heating (see Fig. 9). Achieving these goals may be possible through direct analysis of the linearized Boltzmann equation or application of high-order moment methods.

ACKNOWLEDGMENTS

The simulations of the BGK model were performed using the simulation code developed by G. A. Radtke. The authors are grateful to G. A. Radtke for making his simulation code available and for help with the computations. This work was supported, in part, by the Singapore-MIT alliance.

[1] H. Schlichting, *Boundary Layer Theory* (McGraw-Hill, New York, 1960).
[2] G. N. Patterson, *Introduction to the Kinetic Theory of Gas Flows* (University of Toronto Press, Toronto, 1971).
[3] C. M. Ho and Y. C. Tai, "Micro-electro-mechanical systems and fluid flows," Annu. Rev. Fluid Mech. **30**, 579 (1998).

[4]D. Y. Tzou, *Macro-to-Microscale Heat Transfer* (Taylor and Francis, Washington, DC, 1997).
[5]D. Y. Tzou, J. E. Beraun, and J. K. Chen, "Ultrafast deformation in femtosecond laser heating," ASME J. Heat Transfer **124**, 284 (2002).
[6]A. M. Radhwan and D. R. Kassoy, "The response of a confined gas to thermal disturbance: Rapid boundary heating," J. Eng. Math. **18**, 133 (1984).
[7]J. F. Clarke, D. R. Kassoy, and N. Riley, "Shock waves generated in a confined gas due to rapid heat addition at the boundary. II. Strong shock waves," Proc. R. Soc. London, Ser. A **393**, 331 (1984).
[8]Y. Sone, "Effect of sudden change of wall temperature in rarefied gas," J. Phys. Soc. Jpn. **20**, 222 (1965).
[9]L. Lees, "Kinetic theory description of rarefied gas flow," J. Soc. Ind. Appl. Math. **13**, 278 (1965).
[10]M. Perlmutter, "Analysis of transient heat transfer through a collisionless gas enclosed between parallel plates," Mech. Eng. (Am. Soc. Mech. Eng.) **89**, 76 (1967).
[11]D. C. Wadsworth, D. A. Erwin, and E. P. Muntz, "Transient motion of a confined rarefied gas due to wall heating or cooling," J. Fluid Mech. **248**, 219 (1993).
[12]A. Manela and N. G. Hadjiconstantinou, "On the motion induced in a small-scale gap due to instantaneous boundary heating," J. Fluid Mech. **593**, 453 (2007).
[13]A. Manela and N. G. Hadjiconstantinou, "Gas motion induced by unsteady boundary heating in a small-scale slab," Phys. Fluids **20**, 117104 (2008).
[14]N. G. Hadjiconstantinou, "The limits of Navier–Stokes theory and kinetic extensions for describing small-scale gaseous hydrodynamics," Phys. Fluids **18**, 111301 (2006).
[15]S. Stefanov, V. Roussinov, and C. Cercignani, "Rayleigh–Bénard flow of a rarefied gas and its attractors. I. Convection regime," Phys. Fluids **14**, 2255 (2002).
[16]A. Manela and I. Frankel, "On the Rayleigh–Bénard problem in the continuum limit: Effects of temperature differences and model of interaction," Phys. Fluids **17**, 118105 (2005).
[17]A. Manela and I. Frankel, "On the compressible Taylor–Couette problem," J. Fluid Mech. **588**, 59 (2007).
[18]T. M. M. Homolle and N. G. Hadjiconstantinou, "A low-variance deviational simulation Monte Carlo for the Boltzmann equation," J. Comput. Phys. **226**, 2341 (2007).
[19]G. A. Radtke and N. G. Hadjiconstantinou, "Variance-reduced particle simulation of the Boltzmann transport equation in the relaxation-time approximation," Phys. Rev. E **79**, 056711 (2009).
[20]E. Yariv and H. Brenner, "Flow animation by unsteady temperature fields," Phys. Fluids **16**, L95 (2004).
[21]S. Chapman and T. Cowling, *The Mathematical Theory of Non-Uniform Gases* (Cambridge University Press, Cambridge, 1970).
[22]P. L. Bhatnagar, E. P. Gross, and M. Krook, "A model for collisional processes in gases I: Small amplitude processes in charged and in neutral one-component systems," Phys. Rev. **94**, 511 (1954).
[23]Y. Sone, *Molecular Gas Dynamics: Theory, Techniques, and Applications* (Birkhäuser, Boston, 2007).
[24]G. Bird, *Molecular Gas Dynamics and the Direct Simulations of Gas Flows* (Clarendon, Oxford, 1994).
[25]For example, in the simulations of Sec. V, the physical flow velocity is given by $u^*=u\epsilon \mathrm{St}\sqrt{RT_0}$, where $\epsilon,u\ll 1$ (see Figs. 1–4). Given the difficulty associated with resolving velocities that are small compared to the speed of sound (Ref. 18), simulation of $\mathrm{St}\lesssim 10$ flows using DSMC requires a very large number of samples.
[26]Identical results can be obtained by expanding A and B in Eq. (5.4) in powers of St and Re, substituting into the general solution (5.1) and Eqs. (5.6)–(5.8) and taking the small Strouhal expansions of r_{s_1} and r_{s_3} in Eq. (5.3).